Towards joint communication and sensing (Chapter 4)

Citation for the original published paper (version of record):
Cosmas, J., Ali, K., Araújo, M. et al (2023). Towards joint communication and sensing (Chapter 4). Towards Sustainable and Trustworthy 6G: Challenges, Enablers, and Architectural Design: 121-158. http://dx.doi.org/10.1561/9781638282396.ch4

Chapter 4

Towards Joint Communication and Sensing

By John Cosmas, et al.[1]

DOI: 10.1561/9781638282396.ch4

Published in *Towards Sustainable and Trustworthy 6G: Challenges, Enablers, and Architectural Design* by Ömer Bulakçı, Xi Li, Marco Gramaglia, Anastasius Gavras, Mikko Uusitalo, Patrik Rugeland and Mauro Boldi (eds.). 2023. ISBN 978-1-63828-238-9. E-ISBN 978-1-63828-239-6.

Suggested citation: John Cosmas, *et al.* 2023. "Towards Joint Communication and Sensing" in *Towards Sustainable and Trustworthy 6G: Challenges, Enablers, and Architectural Design*. Edited by Ömer Bulakçı, Xi Li, Marco Gramaglia, Anastasius Gavras, Mikko Uusitalo, Patrik Rugeland and Mauro Boldi. pp. 121–158. Now Publishers. DOI: 10.1561/9781638282396.ch4.

now
the essence of knowledge

1. The full list of chapter authors is provided in the Contributing Authors section of the book.

Localization of user equipment (UE) in mobile communication networks has been supported from the early stages of 3rd generation partnership project (3GPP). With 5th Generation (5G) and its target use cases, localization is increasingly gaining importance. Integrated sensing and localization in 6th Generation (6G) networks promise the introduction of more efficient networks and compelling applications to be developed.

Many use cases such as factories of future, healthcare, autonomous vehicles, energy, and urban environment require not only low latency, low jitter, and high availability data transmission applications that include closed-loop control on one side and ultra-high data rate communication applications that include video or large sensor data traffic on the other side, but also localization accuracy with a precision of up to 1 mm that would be an essential enabler for opening up a lot of new applications.

5G localization systems utilize received signal strength (RSS), time-of-arrival (ToA), and angle-of-arrival (AoA) technologies with sub-6 GHz, mmWave, and optical wireless communication (OWC) for estimating position of UE, whereas simultaneous localization and mapping (SLAM) systems could combine the utilization of communication technologies such as orthogonal frequency division

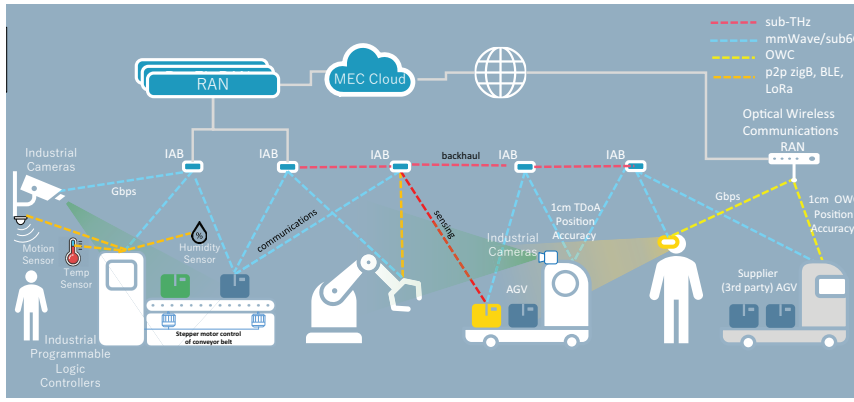

Figure 4.1. Expected sensing use cases in an Industry 4.0.

multiplexing (OFDM), orthogonal time frequency space (OTFS), OTFS-like, or frequency-modulated continuous wave (FMCW) modulation with sensing technologies such as terahertz (THz) beam technologies to sense point cloud of its environment by identifying landmarks for estimating position of UE. Essentially, the plurality of multiple-sensing technologies and multiple-sensing nodes will ensure the continued ability to obtain localization of UE despite the occurrence of any obstructions.

Figure 4.1 depicts expected sensing use cases in an Industry 4.0 setting, where, e.g., the localization accuracy requirement for automated guided vehicles (AGVs) and collaborative drones is 1 cm every 1 s, for augmented reality (AR) headsets it is 1 mm every 100 ms, for collaborating mobile robots (cobots) it is 1 mm with cycle time of motion control function of 1 ms, synchronicity of 10 ns, and for motion, temperature, humidity, etc., sensors is 10 cm every 1 to 10 s, whilst all require the provision of localization with 99.99% reliability. The motivation for using 6G mobile networks for localization as opposed to a dedicated radar/LIDAR system is the pervasiveness of mobile networks means that they can be applied universally and can employ the economies of scale to produce new and cheaper pervasive services that use high accuracy localization. The best LIDAR systems can obtain a precision from between 0.5 cm over 200 m (Ouster OS1) [1] to 2 cm over 400 m (Ouster OS2) [2] accuracy, which is an indication of what accuracy can be expected from a 6G communication and sensing system.

The sensing stratum uses the control plane for issuing reference signals for measuring RSS, ToA, and AoA for scheduling measurement frequency and accuracy for UE, the management plane for providing administrative data for computing UE position from distance measurements, and the vertical application Application Programming Interface (API) for accessing the UE position, see Figure 2.3 in Chapter 2.

In particular, highly advanced industrial environments will present significant challenges even for 5G specifications (up to Release 18 3GPP specifications), spanning congestion, interference, security and safety concerns, high power consumption, restricted propagation, poor location accuracy within the radio, and core backbone communication networks for the massive IoT use cases, especially inside buildings. 6G is preparing a new solution consisting of a combination of artificial intelligence (AI) methods with new communication technologies, potentially extending to OWC and THz to perform resource allocation over and beyond massive machine-type communications and to enhance performance with regard to capacity, reliability, latency, and localization accuracy. Examples of localization in industry are its use with video guides for facilitating maintenance of equipment and graphics superimposed on AR field of view of a factory or warehouse scene for the accurate location of electric, gas, and pneumatic facilities; mobile service robots in airports for physically guiding passengers through airport; and for AGV robots for carrying passenger luggage between baggage handling conveyor belt locations in airports [3].

6G and its visionary scenarios continue this trend and look at localization that is even more accurate and has even stricter latency requirements [4]. 6G SLAM will require multiple access technologies, such as sub-6 GHz, mmWave, sub-THz for RSS, Time Difference of Arrival (TDoA), and AoA localization, combined with sub-6 GHz sensing to produce a point cloud for producing a digital twin for updating the digital twin for obtaining location from environmental landmarks. Computational offloading such as on a multi-access edge computing (MEC) cloud is required for producing location from all these technologies using AI, for example, to recognize location from landmarks and artificial intelligence/machine learning (AI/ML), for example, to Kalman filtering to predict position and trajectory from measurements. This will provide novel and enhanced sensing and localization services leveraging on the positioning information of the users and their surroundings, for instance for merged reality or digital twins. For this, 6G will primarily act as a connector between the sensors and the users, e.g., with sensor fusion, where sensor data from different modalities are combined. However, 6G may also play a role in storing, aggregating, and analysing the sensor data before providing the mapping information to the user.

Another aspect of positioning and sensing in 6G is the possibility to incorporate the sensing data into the network operations. With an accurate map of the surroundings, the locations of the users and various stationary and moving obstacles, the user mobility, and optimal beam pattern can be predicted, improving the performance and resource utilization.

Finally, the research into 6G engenders a paradigm shift in the radio interface. For the past century, radio waves have been used for either communication

or sensing, i.e., radar. However, as the radio communication begins using higher radio frequencies (>100 GHz), the potential sensing accuracies become viable. By repurposing the radio interface of the mobile network from only communication to joint communication and sensing, the ubiquity of the mobile devices and networks can provide a cost-efficient and widely spread sensing resource that can be used to enhance user services or network operations.

Section 4.1 presents the plurality of multiple sensing techniques to produce extremely accurate sensing information to a user to enhance services using, e.g., sensor fusion, i.e., 6G primarily acts to connect the sensors with user. Section 4.2 presents the plurality of multiple sensing nodes to enhance connectivity. Section 4.3 presents the repurposing of the radio interface to also act as a radar (i.e., Joint Communication and Sensing (JCAS)). All these technologies will ensure the continued localization of UE despite the occurrence of any obstructions.

4.1 Providing Extremely Accurate Sensing

4.1.1 Sub-1 cm Location Accuracy Using Sensor Fusion

Localization of UEs using ToA from sub-6 GHz wireless and RSS from optical wireless infrared techniques can be used to obtain an accuracy of less than 1 cm; however, it is highly dependent on the continuous direct line of sight access between the gNB access points (APs) and the UE. If there is no direct line of sight access to four or more gNB APs, then location ambiguity is introduced, and so other techniques can be used to maintain localization such as dead reckoning from inertial measurement unit (IMU), AoA from received radio signatures, iterative multi-lateration, or position from landmarks. The received radio signatures estimate AoA from more than two APs or AoA and distance from one AP, so that some forms of interim measures for obtaining location can continue to be made. Distance and speed of UE can be estimated using OTFS modulation from one AP due to its operation in the delay and Doppler domain as opposed to using OFDM, which operates in the time and frequency domains. If there is no direct line of sight access to any 6gNB APs, then position from landmarks calculates position from at least four landmarks identified from within point cloud data of a sensed environment obtained, for example, from a 6G sensing/LIDAR system and/or 360-degree image.

4.1.1.1 Distance measurement and localization using AI

3D localization using RSS or TDoA requires line-of-sight (LoS) time of flight (ToF) measurements to picosecond accuracy for estimating distance to mm accuracy from at least four accurately located 6gNB APs; otherwise, inaccuracies and ambiguities are obtained where more than one solution is produced. LoS propagation paths to

each of these APs may not always be available as a result of incidental occlusion from moving objects, so a strategy of providing more, cheaper APs for providing alternative means for obtaining location and alternative methods using fewer APs are required such as AoA, which only requires two APs, since two lines intersect at or close to a point, or one AP and a distance, since a line and a distance define a point on the line.

In order to design such a system, a digital twin was obtained from 3D laser measurements in a real factory, and a ray tracing (RT) model was used to generate a rich data set of point cloud data, which was converted into a Siteviewer or Winprop CAD "digital twin" model, which uses a deterministic methodology to predict radio propagation of THz and mmWave frequencies based on the geometrical theory of propagation (GTP) that takes into account geometrical properties of the environment and propagation parameters such as ToF, direction of arrival (DoA), and direction of departure (DoD) [5].

The beam scheduler implements intelligent beam steering that, using an antenna array, can steer beams from 6gNB RUs to UE locations efficiently based on interpreted channel impulse response (CIR) knowledge of uplink isotropic transmissions from uplink UE. Then, it optimizes the beam direction using reinforcement leaning (RL) to maximize the SINR, and when the path between the transmitter and receiver is broken through an obstruction, it immediately finds and uses alternative secondary paths to steer the beam between the transmitter and receiver by avoiding the obstruction. The optimized beam direction from two BSs can also be used to obtain the location of UE locations.

The beamforming vector is obtained through a deep neural network (DNN) by using predicted digital twin isotropic transmissions from UE in a grid over the coverage area, and the predicted digital twin measured impulse response at each 6gNB RU receiver of four polarized transmissions and received power that acts as input information to train a DNN. Four polarizations were used to have more flexibility in terms of data generation for the training of AI, implying that the more polarizations the better for the AI training.

The beamform codebook index is the set of beamform vectors comprising of steering angles at the receiver of different alternative secondary paths to steer the beam between the transmitter and receiver by avoiding any obstruction. In the absence of a real environment, the beamforming power control and interference coordination are jointly carried out on a digital twin to enhance the performance of the 5G network. The network comprises of serving gNBs and one interfering gNB as shown in Figure 4.2. The deep reinforcement learning-neural network (DRL-NN) is modelled for the downlink scenario in which a gNB is serving a UE. The gNBs are a fixed, known distance apart, and different UEs are uniformly distributed in a particular service area. Also, the users are moving at a fixed speed.

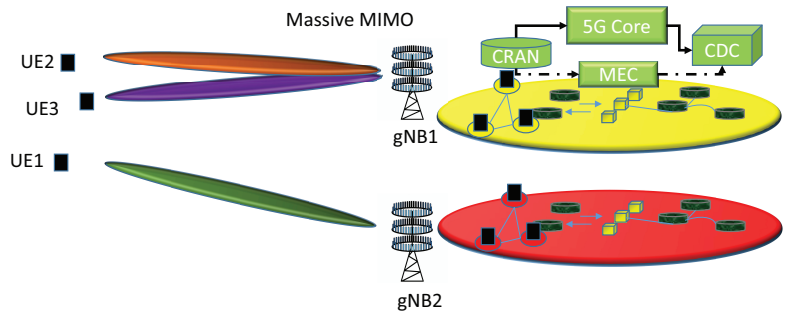

Figure 4.2. Radio beam control.

An UE is served by a maximum of one gNB. Hybrid beamforming for the downlink data transmission is employed to overcome the problem of high propagation loss.

RL is then to optimize the beam direction, whose state space, action space, reward, and learning algorithm are defined in [5]. Initial simulation is performed on MATLAB 2021a siteviewer for radio transmission (RT) using site viewer and simultaneous channel generation [6], but it could equally well have used Winprop, which models more accurate geometries and accommodates more surface properties [5]. The output of RT is fed for channel generation, which in turn produces input for the DNN for training. For RT and channel generation, different users' locations for fixed 6gNB RU positions are considered. Channel parameters vary with respect to varying user locations. Therefore, DNN is trained to different channel parameters, which in turn are dependent on user location. The DNN is trained on python AI module and is trained for efficient beamforming of the data towards the user. Post-training and during the working phase, the system performs beam scanning to obtain the channel parameters based on user locations. Beamforming weights are adjusted from channel parameters to form the beam pointing towards the current user location. In this way, based on the obtained channel parameters, the user locations could be estimated [5]. If a beamformer steers the main beam in a particular direction (θ, φ), then the directional accuracy is defined as $\pm\delta\theta$, $\pm\delta\varphi$ from the maximum signal-to-noise ratio (SNR) of the main lobe. The proposed deep learning integrated reinforcement learning (DLIRL) beamforming has an angle-of-departure (AoD) accuracy towards the UE location with a deviation of $\pm 2^\circ$, whereas RL has a deviation of $\pm 3^\circ$ and DNN's deviation is $\pm 5^\circ$ [6].

4.1.1.2 Distance measurement using TDoA on mmWave Networks

The accurate 3D location of the 5G UE is calculated by the use of ToA measurements from at least four different locations and then exercising triangulation techniques as shown in Figure 4.3. In order to reach the required 1 cm accuracy, it

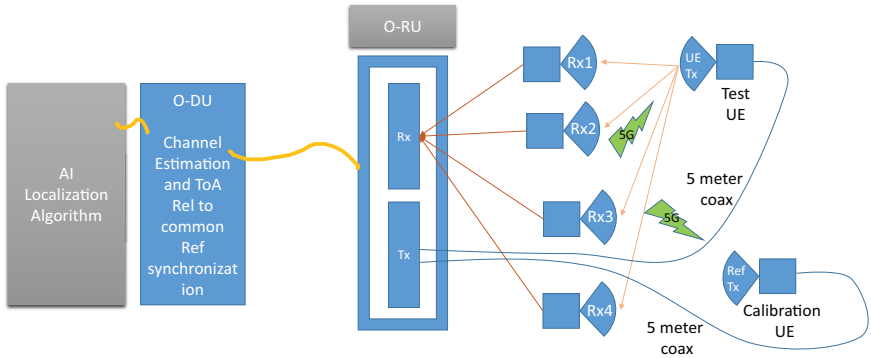

Figure 4.3. Setup for ultra-accurate UE distance measurement.

is required to measure the ToA at accuracy levels of ~33 picoseconds (calculated from 1 cm/speed of light).

The setup that is used to measure the test UE location consists of the O-RU and O-DU and the localization measurement algorithm application installed on an X86-based server. The O-RU is configured in a loop-back mode, which enables it to transmit 5G OFDM pseudo-random noise (PN) signals (Tx) at 3.5 GHz similar to the UE transmissions. These Tx signals are connected via coax to two patch antennas that simulate the test UE and the reference UE. The reference UE is a UE with a known location that is used to calibrate the accurate test UE location measurement. The test antenna is located on a scanner that can accurately move its position to new locations in space. The 5G signals transmitted over the air at 3.5 GHz by the test UE and the reference UE patch antennas are received by the O-RU receiver (Rx) via four different Rx antennas located in the four corners of the ceiling of the measurement room. The O-RU will continuously measure the ToA of the 5G signals coming from the test UE and the reference UE with a resolution of 0.3 ps (corresponding to 0.1 mm) and transfer the results to the O-DU that stores them on agreed memory sharing register. A localization algorithm reads the ToA registers and calculates the test UE location. Following the successful test UE location described herein, the test UE might be replaced by a commercial UE [7].

Some initial results, which are illustrated in Figure 4.4, show that although the measurement samples have been measured with a resolution of a timetic of 0.33 ps or 0.1 mm, the samples are approximately normally distributed about the mean of 69516 timetics or 6.9516 m. The 95% confidence interval falls within ±2 times the stdev = 833 × 2 = 1666 timetics = 16.66 cm about the mean, which can be considered as a measure of accuracy. It is assumed that the mean of the measurements represents the true distance that is being measured, which was not provided in these initial results. A Kalman filter is an effective method for

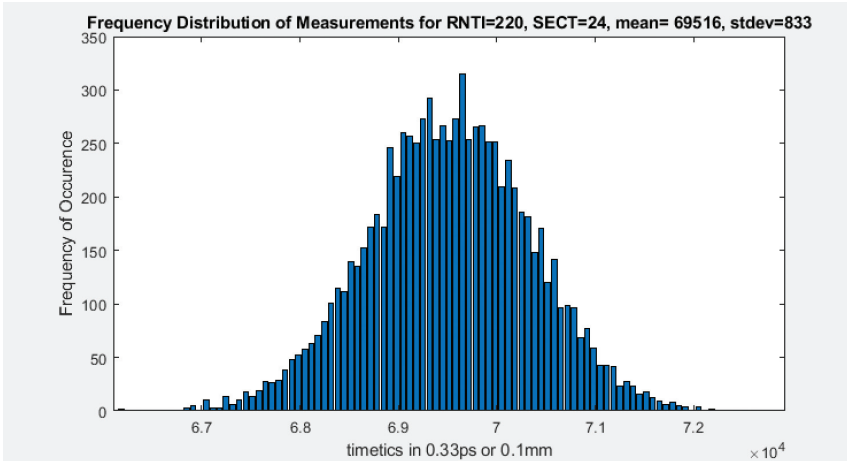

Figure 4.4. Frequency distribution of measurements for RNTI = 220, SECT = 24.

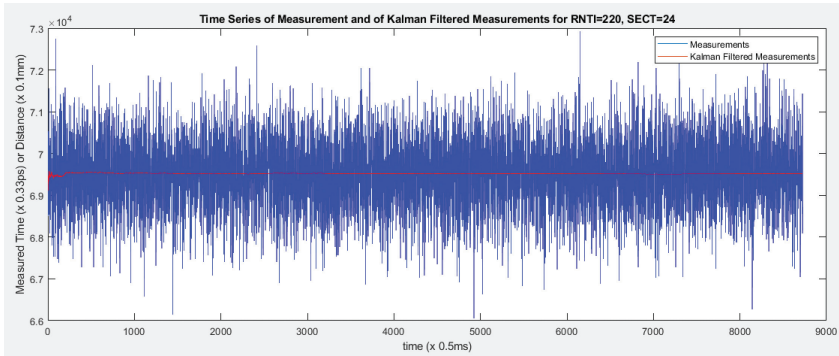

Figure 4.5. Time series of measurement and Kalman-filtered data for RNTI = 220, SECT = 24.

reducing normally distributed noise from measurement results, which when applied reduces the 95% confidence interval to ±2 times the stdev = 13.74 × 2 = 27.48 timetics = 2.748 mm about the mean, as shown in Figure 4.6, which is considered as a measure of accuracy of the filtered measurement data. The time series of the overall measurement results and Kalman-filtered measurement results are shown in Figure 4.5. Note that RNTI = 220 refers to the calibration UE, and Sect = 24 refers to the portion of spectrum being used for the measurements, as shown in Figure 4.5. These initial results seem to be sufficient to meet <1 cm accuracy but need further improvement to meet <1 mm accuracy.

4.1.1.3 Distance measurement using RSS on OWC networks

If obtaining location from 5G sub-6 GHz or mmWave communications is made difficult, for example, as a result of highly reflective metallic scatterers in the

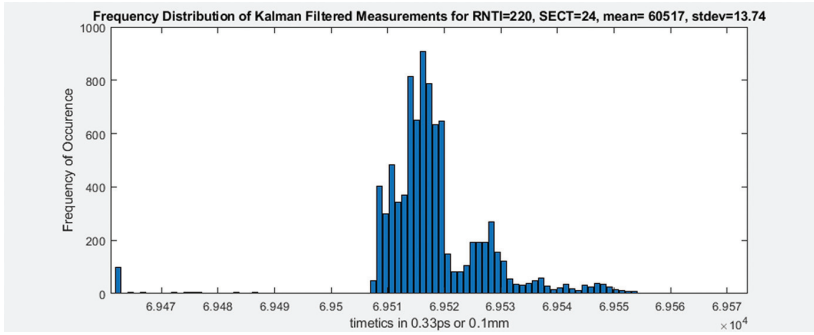

Figure 4.6. Frequency distribution of Kalman-filtered measurement for RNTI = 220, SECT = 24.

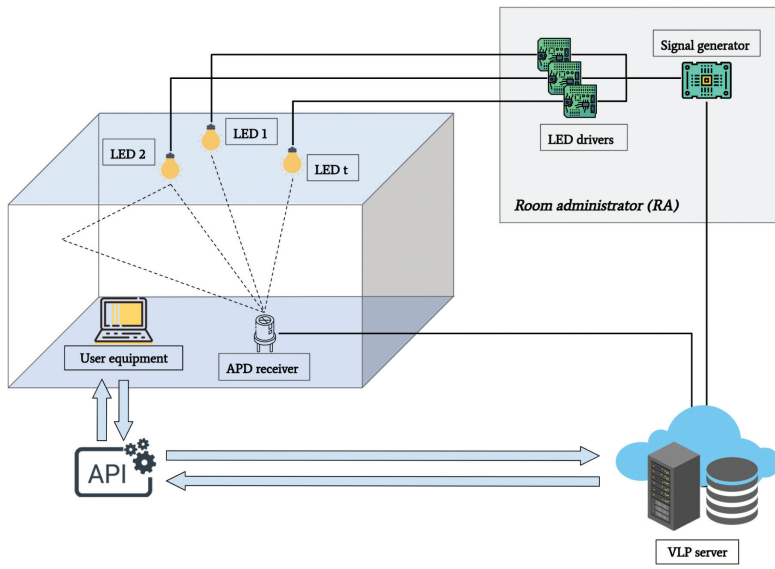

Figure 4.7. OWC position testbed.

coverage area, then RSS of an OWC communications system can be used as an alternate method for estimating position.

The OWC position testbed contains three main components for visible light positioning (VLP) LED or IR LED measurement campaign, as shown in Figure 4.7.

1. Location server: Including three parts: (1) LED control unit, (2) received signal collection unit, and (3) positioning unit. In an LED control unit, it is connected with an Arduino board, which has been set up to control LEDs in advance, including the LED switch settings and LED frequency settings. These settings can be used to control on/off of LEDs and change the frequencies of LEDs. When the VLP server receives setting change requests

from API, it will change settings of the LEDs according to the user's requests. In the received signal collection unit, it collects received signal data from APD receiver connected by a USB port, which can be downloaded by user through API. In the positioning unit, user can upload the received signal data file to execute positioning algorithm. Users can use the files obtained in the previous unit or upload them themselves. The positioning algorithm used in this server is traditional trilateration received signal strength indication (RSSI) algorithm. The output of the algorithm is the estimated coordinate of the receiver.

2. LED transmitter module: Including LED and its corresponding drivers. Every LED has to be driven by an LED driver in order to convert the power supply from 220 V into a suitable value and switch the frequency of LED.
3. Avalanche photodiode (APD) receiver: A highly sensitive semiconductor photodiode detector used to measure and collect received light signals. The received data are transmitted to the VLP server through the USB cable.

Some results in comparing with traditional RSSI-based VLP algorithm are shown in Figure 4.8. Two figures represent the values of ε when the orientation of the receiver was randomly in the range of $[-3°, 3°]$ and $[-5°, 5°]$, respectively. The results are very similar, which reflects that the algorithm has good immunity to changes in receiver angle.

Firstly, in Figure 4.8(a), when the traditional algorithm was employed and the orientation of the receiver θ was in $[-3°, 3°]$, values of ε were plotted using blue crosses for each measurement. They were mostly scattered between 0.25 and 0.35 m, and the average deviation is 0.31 m. It could be observed that even though the angle of the receiver θ was the same value, the value of ε is different for different measurements. In other words, not only did the estimate of the distance between the transmitter and the receiver always have a large deviation, but the deviation was also difficult to determine.

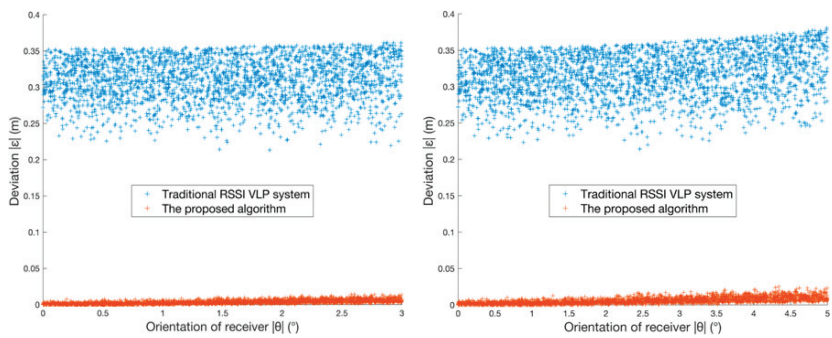

Figure 4.8. Deviation of the proposed algorithm and traditional RSS-based VLP algorithm with a variation of receiver angle (a) $\theta \in [-3°, 3°]$ and (b) receiver angle $\theta \in [-5°, 5°]$.

Afterwards, when the proposed algorithm was employed, the values of ε were scattered using red crosses. Compared with blue crosses, red crosses were much closer to the x-axis: this means that the value of ε was closer to 0. Indeed, the average of ε decreased to 3.5×10^{-3} m, and the maximum and minimum values of ε declined from 0.36 to 0.01 m, and from 0.2133 m to 1.33×10^{-5} m, respectively. Moreover, the distribution of red crosses was more compact: on the one hand, when the value of θ became the same, the values of ε calculated by different measurements were not very far from each other; on the other hand, the value of ε did not change greatly according to the change of θ.

Therefore, it could be inferred from the distribution of blue and red crosses that, in general, our proposal led to less deviation and a more concentrated distribution than traditional methods. As a result, estimated distances between transmitters and receivers would be closer to their real distances by using our proposal. Furthermore, it could be boldly predicted that it could lead to lower positioning errors (PEs).

This trend is also evident in Figure 4.8(b). When the traditional algorithm was employed and the orientation of the receiver θ was in $[-5°, 5°]$, blue crosses were mostly scattered between 0.25 and 0.4 m, and the average deviation was 0.3103 m. Compared to the situation of θ in $[-3°, 3°]$ in Figure 4.8(a), the average deviation has barely changed, but the distribution of their values was more spread out in Figure 4.8(b). It can be inferred that the deviation of the distance between the transmitter and the receiver caused by the random orientation of the receiver became larger and less predictable as the range of values of θ expands.

The CDF of positioning results is shown in Figure 4.9. 98.81% of the total results had the PE less than 10 cm, which means almost all of the receiver's positions could be accurately estimated.

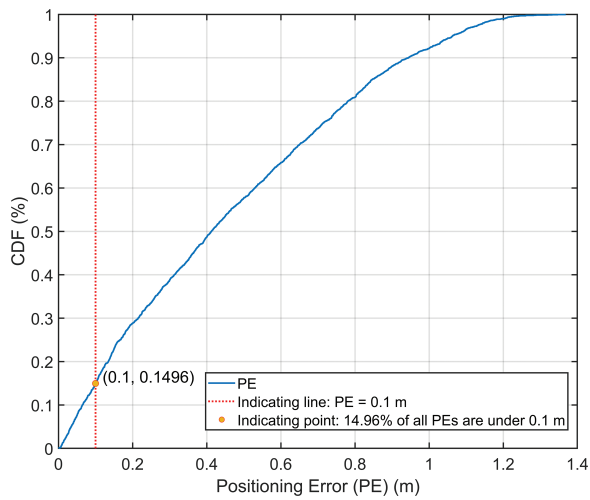

Figure 4.9. CDF of positioning results of the proposed algorithm and traditional RSS VLP algorithm in different receiver's orientation: using the proposal when $\theta \in [-5°, 5°]$.

4.1.1.4 Distance measurement using OTFS modulation

The 5G air interface and associated modulation have to support a number of diverse requirements and use cases (e.g., eMBB, high-speed use cases, mMTC, etc.), as detailed in many publications. The associated modulation waveform would then have to exhibit high performance in many diverse scenarios of high or low Doppler, delay spread, carrier frequency, etc. This is possible if the modulation scheme takes full advantage of the fading multipath nature of the channel and extracts the full diversity present in the channel in all dimensions of time, frequency, and space. Such a flexible waveform can serve as an integral part of a flexible air interface and associated core network. Therefore, researchers have recently introduced a novel modulation technique called OTFS [8], which may be useful for obtaining position of fast-moving UEs with high Doppler. It has been shown recently that OTFS arises as a well-suited modulation for the time and frequency selective fading channel. OTFS characterizes the Doppler-induced time-varying nature of the wireless channel and parameterizes it as a 2D impulse response in the delay-Doppler domain.

OTFS works in the delay Doppler domain rather than the time-frequency domain as shown in Figure 4.10. The delay Doppler domain representation of the channel converts the time-variant channel to the time-invariant channel, as shown in Figure 4.11. In addition to the OTFS diversity gains mentioned above, we have additional benefits of low reference signal overhead, enhanced channel state information (CSI) quality, and MIMO bit error rate (BER) performance of fast-moving UEs, as shown in Figure 4.13.

Because of the added advantages of OTFS over OFDM, the OTFS is an efficient way of estimating the localization via computation of ToA.

The above Figure 4.12 shows how a UAV can be efficient in locating the user in need via employing the OTFS for estimating an accurate ToA.

From the BER analysis for the OTFS and OFDM modulated signals shown in Figure 4.13, the comparative analysis of the OTFS and OFDM modulated signals

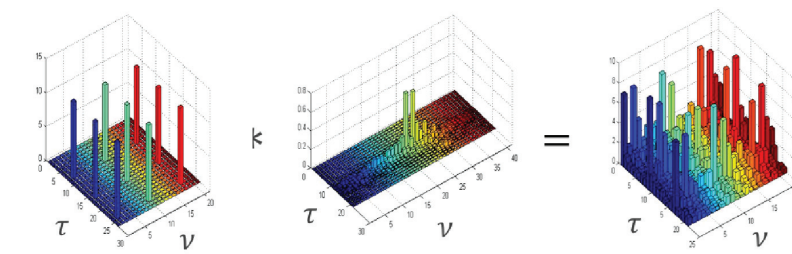

Figure 4.10. Transmitted OTFS QAM symbols and corresponding received symbols via delay Doppler channel.

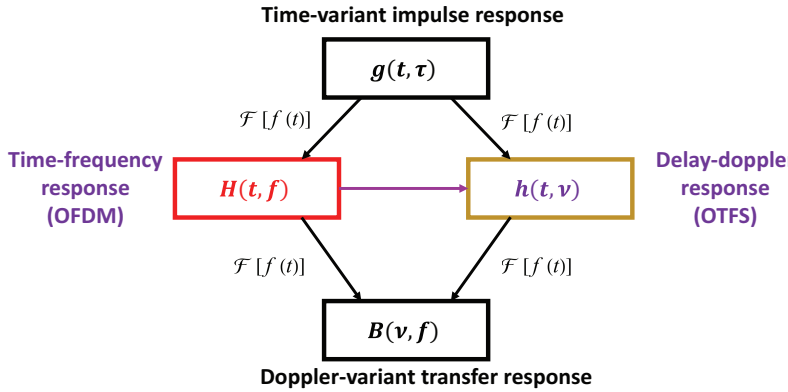

Figure 4.11. Different representations of linear time variant (LTV) wireless channels.

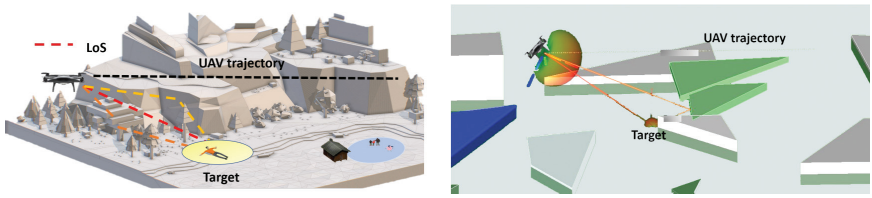

Figure 4.12. UAV with OTFS employed for the user localization.

for fast-moving UE (where the UE is moving at a constant speed of 28 km/h) can be visualized. The BER for OTFS-modulated signal is lower because its performance is not degraded even with the fast motion of the UE, and the bit error and bit loss are less as compared to the conventional OFDM. Thus, OTFS may be able to more reliably estimate the distance of UEs moving at a fast speed.

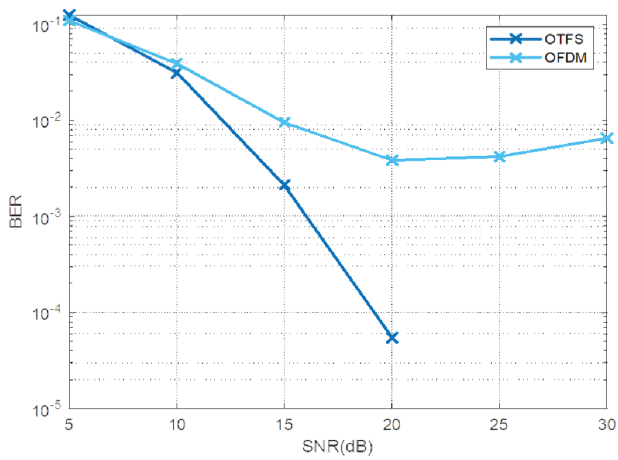

Figure 4.13. BER comparison of OTFS and OFDM when UE is moving at a constant speed of 28 km/h.

4.1.1.5 Distance and angle measurements using physically large arrays

To give an outlook towards the capabilities of large aperture arrays, a measurement-based analysis of beamforming and channel estimation is performed, targeted at positioning applications. The initial results are obtained using spherical-wave beamforming applied to data recorded using a (synthetic) large uniform rectangular array (URA), representing a large base station (BS) that is positioned along a wall in an indoor environment. The results are visually compared with super-resolution channel estimation results obtained when splitting the large URA into small sub-arrays. The channel measurements were recorded with a vector network analyser (VNA), with the synthetic arrays formed using mechanical positioners with a positioning accuracy below 1 mm.

Exploiting the full array aperture requires spherical-wave beamforming and perfect calibration of the full array, which can be difficult to achieve for thousands of array elements. The advantage of using the full available data is the superior resolution that can be achieved, allowing focusing power towards small spatial regions [9, 10], e.g., $\lambda = 2.16$ cm, for a carrier frequency of $f_c = 6.95$ GHz, is shown in Figure 4.14. The marginal spectra include modelled components that are computed from a geometric floorplan in combination with an image source model up to second order. In combination with the large aperture, a large signal bandwidth of BW = 3 GHz is used to show the optimum case regarding the achievable resolution. From the sub-figures, while direct paths and first-order reflections are well represented by the model, second-order reflections, which might no longer be visible over the full array, are not well associated with modelled components.

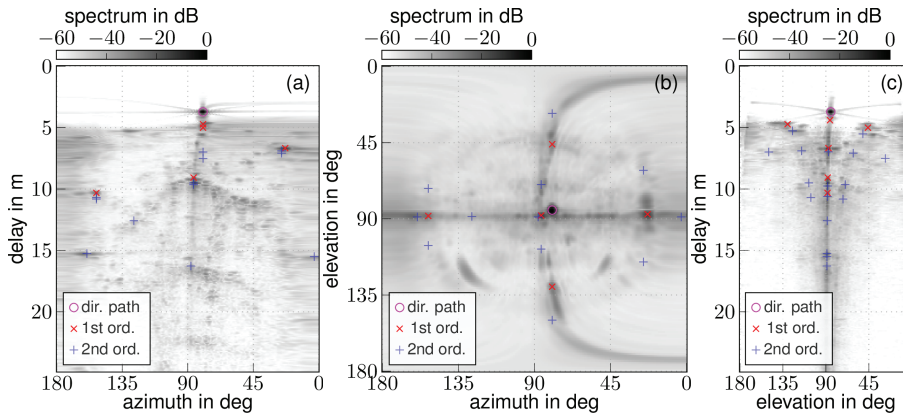

Figure 4.14. Spherical wave beamformer spectra for an exemplary LOS position in a medium-sized indoor environment. In the analysis, we use the full measurement bandwidth and all (synthetic) array elements. In the azimuth-elevation power spectrum shown in (b), 0 deg azimuth points towards a window in the environment and 0 deg elevation towards the ceiling.

Parametric approaches such as super-resolution channel estimation algorithms can achieve a high level of performance under the assumption that the channel is composed of discrete components that are parameterized in terms of, e.g., arrival times or angles. The separation into sub-arrays allows to make use of classic array processing assumptions, which are not feasible for application to the full array data, drastically improving the requirements for computational resources. Results obtained when applying a sparse Bayesian learning (SBL)-based channel estimation algorithm (described in [11]) to (4 × 4)-subarrays and B = 500 MHz of signal bandwidth are shown in Figure 4.15, as angle spectra (a), residual angle spectra after subtracting component estimates (b), and time-domain residual signals after subtracting the obtained component estimates (c). In Figure 4.15(a) and (d), the size of the markers represents the estimated amplitude, and the colour indicates whether a component was associated with a modelled component (cyan) or not (magenta). This association is performed by using an optimal sub-pattern assignment-based data association algorithm, which allows to associate estimated components to modelled components and thereby accounts for the varying visibility of multipath components (MPCs). While using only a fraction of the array elements and bandwidth, the obtained estimates still correspond well with the modelled MPCs. At the same time, the varying visibility can be accounted for, which will be an important

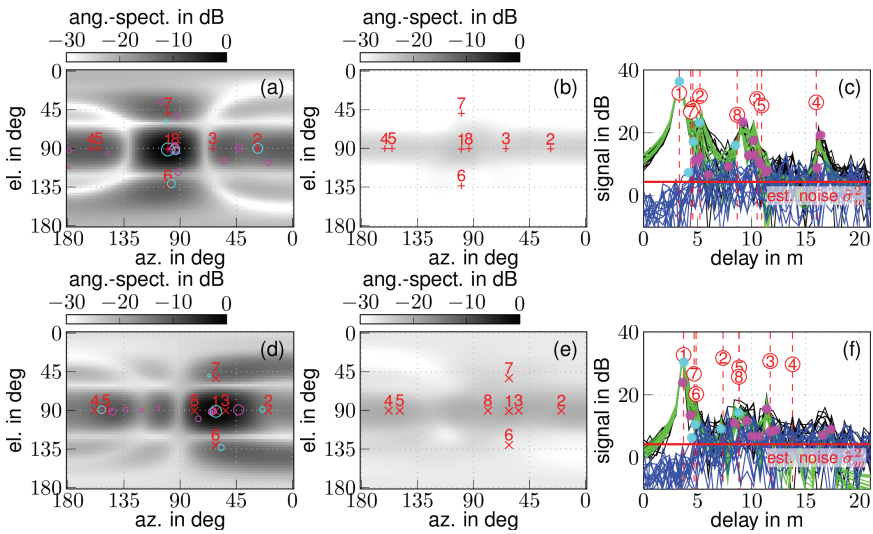

Figure 4.15. Channel estimation results using an SBL-based algorithm, showing estimated components over the angle-spectrum, residual angle-spectrum, and residual time-domain signals. Results are shown for (4 × 4) sub-arrays with 500 MHz bandwidth and for a subarray closest to the window (a, b, c) and farthest from the window (d, e, f). Component estimates are shown as magenta and cyan circles with the latter indicating association to a modelled environment feature (numbered 1–8), with 1 representing the direct path and 2 a window reflection.

aspect for multipath-based positioning and environment learning. Note the consistent changes that are visible in the modelled as well as estimated components, comparing the two subarray positions that are closest to the window (top row in Figure 4.15) and farthest from the window.

While analysis of the measurements performed has shown the effects of visibility as well as the spatial consistency of MPCs, without efficient fusion of subarrays, it will be difficult to achieve a similar performance compared to a large and fully coherent array. The next step will be the derivation of theoretical performance limits, e.g., in terms of the Cramer-Rao lower bound or similar, giving insight into system parameters such as signal bandwidth and the geometric distribution of sub-arrays. Of special interest will be the effect of imperfect phase or clock-synchronization between the subarrays, which is expected to be the main limiting factor to achieve the same performance as a fully coherent array.

4.1.1.6 Precise localization with the aid of synchronization signals and CIR

4.1.1.6.1 Introduction

Instead of adding an extra overload to the communication systems, one can rely on the mechanisms already in place to perform precise localization. In particular, approaches based on TDoA and ToA require the nodes not only to be synchronized with each other, but also to exchange localization-specific signals. However, the synchronization signals exchanged among the nodes for the purpose of synchronization as well as other sources of information such as CIR and AoA estimation, which are not primarily foreseen for localization purposes, can be utilized to precisely estimate the position of a UE.

In [12], the principles of network synchronization have been presented, which paves the way for an accurate mobile UE localization with the aid of synchronization signals, i.e., time stamps. In particular, a Bayesian recursive filtering (BRF)-based mobile unit (MU) joint synchronization and localization (sync&loc) approach is developed where Taylor expansion is utilized to linearize the non-linear relation between the measurements, i.e., time-stamp exchange and AoA, and the position parameters. While linearized BRF (L-BRF) can partially mitigate the destructive impact of non-linearities in the measurements, in addition to the covariance matrix underestimation, they are likely to diverge if a reliable estimate of the initial state is not available [13]. A promising approach, on the one hand, to avoid such shortcomings of L-BRF and, on the other hand, to boost the accuracy of position estimation, is estimating the prediction, measurement likelihood, and posterior distributions using particle Gaussian mixture (PGM) filters introduced in [14]. Specifically, in this approach, instead of a single Gaussian function, each

distribution is approximated with a sum weighted of Gaussian functions or Gaussian mixtures [15]. Nevertheless, the problem that immediately arises when using PGM filters is dimensionality, rendering the approach computationally expensive for multi-variable estimations. To overcome this drawback, a hybrid parametric and particle-based approach was employed, which capitalizes on the linear relations in the measurements to reduce the dimensionality.

Here, based on [16], a DNN-assisted particle filter (PF)-based (DePF) joint sync&loc algorithm is proposed that draws on the CIR to estimate the AoA (using multiple signal classification (MUSIC) algorithm [17]) and to determine the link condition, i.e., LoS or NLoS, using a pre-trained DNN, thereby excluding the erroneous measurements to enable a more precise parameter estimation. It then estimates the joint probability distribution of MU's clock and position parameters using the PGM filter. The dimension of the PGM filter is then reduced by revealing and exploiting the existing linear sub-structures in the measurements, thereby tackling the dimensionality problem.

There are, however, several preliminaries for the PGM filter to return an accurate estimation of the MU's clock and position parameters. In addition to the time-stamp exchange mechanism explained in [12], as mentioned above, AoA using the MUSIC algorithm and DNN-based NLoS identification are the prerequisites for the DePF algorithm. The former increases position estimation accuracy, while the latter prevents the PGM from diverging.

4.1.1.6.2 NLoS identification, AoA, and CIR

The capability to estimate CIR is highly ubiquitous among APs. Therefore, relying on the CIR to develop a localization algorithm appears to be a realistic approach. The AP-UE CIR is a rich source of information about the condition of the communication link, e.g., whether the channel is LoS or NLoS, and the location of the UE. More precisely, the former is crucial to know when estimating the latter, as is the accuracy of the distance or time, and AoA measurements significantly decline if conducted under NLoS conditions.

Figure 4.16 shows the architecture of the DNN deployed for NLoS identification. We have utilized such a network in [18] to identify the link condition in indoor environments. The input layer has one channel fed with N samples, i.e., the magnitude of the CIR. The number of hidden layers and neurons in each hidden layer is set to l_H and n_H, respectively. The rationale to rely on when selecting these numbers is that, according to [19], any classifier function can be realized by two hidden layers, i.e., currently there is no theoretical reason to use more than two. However, the lack of evidence does not imply that the DNNs with more hidden layers do not improve the classification accuracy. It rather suggests that the number of required hidden layers does not follow a well-established logic and is

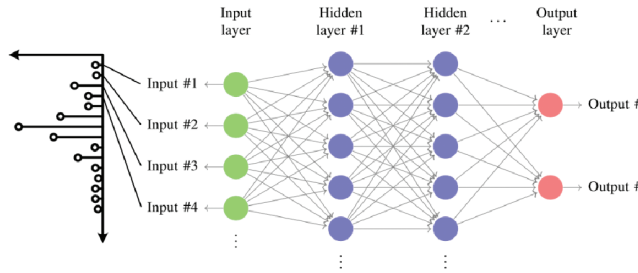

Figure 4.16. The DNN employed for NLoS identification. It has $l_H = 2$ hidden layers with n_H neurons and two output neurons [16].

mainly determined by a trial-and-error process. Therefore, for the algorithm proposed in this work, we empirically determine the number of hidden layers that delivers the best performance. Furthermore, as a rule of thumb, the number of neurons is suggested to be between the number of inputs and that of the outputs to prevent under/overfitting. Let the output probability vector of the DNN be $[1 - \hat{p}_{nlos}, \hat{p}_{nlos}]$, where $\hat{p}_{nlos}$ denotes the probability of the CIR being corresponded to an NLoS link. For the NLoS identifier, we seek to train the DNN such that the output probability vector is as close as possible to the [1,0]/[0,1] for the LoS/NLoS CIRs. In other words, from the optimization point of view, we aim to design a loss function whose output is small when the DNN returns the correct vector and is large otherwise. It turns out that the function that possesses the above-mentioned property is the logarithmic function [20]. The loss function is known in the literature as the binary cross-entropy loss function. The goal of training is then to adjust the weights of the neurons such that the binary cross-entropy loss function is minimized. Finally, when the trained DNN is employed in the context of joint synchronization and localization algorithm, the decision on the link condition is fed into the algorithm using a binary parameter, which is set to one when $\hat{p}^i_{nlos} > 0.5$ and zero otherwise. The CIR fed into the DNN to identify the link condition can be treated as an input signal to the state-of-the-art AoA algorithms such as MUSIC or Estimation of Signal Parameters via Rational Invariance Techniques (ESPRIT) to obtain the AoA. We do not mention the details of these algorithms here, as rich literature on these algorithms is available online. In what follows, we elaborate on how PGM filters fuse the above-mentioned pieces of information to reach an estimation of clock and position parameters.

4.1.1.6.3 Particle Gaussian mixture filter

The data obtained from the synchronization signals, i.e., time-stamps, the channel condition obtained by means of DNN, and the AoA estimated using the CIR can be fused using PGM filters to estimate the location and clock parameters of an UE.

The idea underpinning PGM filters is to approximate the posterior PDF by the sum of weighted Gaussian density functions (GDFs) [15] as shown in Figure 4.17.

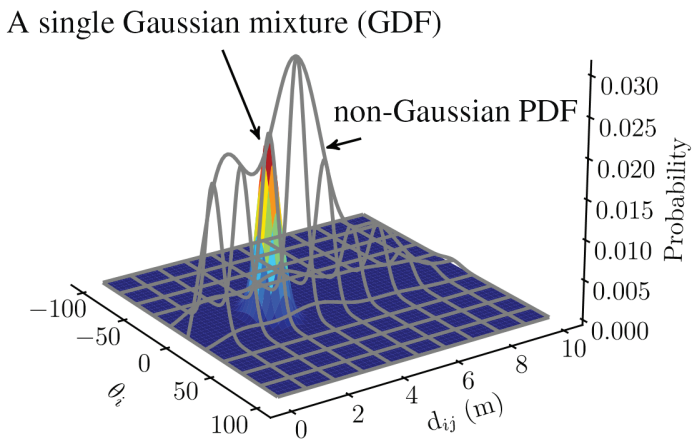

Figure 4.17. An example distribution of the clock and position parameters. θ_i denotes the clock parameters and d_{ij} represents the position parameters [16].

Considering the time-stamp mechanism introduced in [12], we can conclude that the clock parameters, on the one hand, are linearly dependent on the time-stamps and, on the other hand, do not depend on the position parameters. This suggests that, although the likelihood of the measurements is not Gaussian distributed in general, it is indeed Gaussian across the clock parameters. By capitalizing on the linear Gaussian substructures in the model, the state dimensions are kept low.

Consequently, the GDFs can be employed only across the position parameters, transforming the structure of the posterior distribution into the multiplication of a single GDF across the clock parameters and the sum of multiple weighted GDF across the position parameters (visualized in Figure 4.17). Such a structure not only lays the ground for the hybrid parametric and particle-based implementation of BRF-based joint sync&loc estimation but also dramatically reduces the computational burden.

4.1.1.6.4 Takeaways

As mentioned in the previous subsections, synchronization signals, i.e., time stamps and CIRs can be utilized to perform precise localization. In particular, we can employ PGM filters in a hybrid parametric and particle manner to track the clock parameters of a UE and estimate its position. Such a technique does not require an exchange of any localization-specific signal and relies only on the pre-existing signal exchange mechanisms.

4.1.1.7 MEC cloud database and server for localization and mapping data fusion

SLAM achieves the purpose of simultaneous positioning and map construction based on combination of self-perception LIDAR-like sensing data combined with localization data. These data are necessarily captured by sensors and collated in a database on which processing can be performed for the purposes of different applications, and in particular location estimation applications, an example of which is now presented below. RSS OWC distance measurements from UEs, TDoA mmWave distance measurements from 6G access nodes, and AoA direction measurements from 6G access are recorded on MEC location database VNF and processed by a location server VNF to produce a data fusion estimate of the location of UEs that is stored on the Location Database VNF for access by network and user applications. Data fusion combines estimates of position from mmWave OWC RSS, TdoA, and AoA position measurements using the Kalman filter machine learning algorithm to obtain a more accurate position estimate that compensates for the different sampling times of the different distance and direction measurements.

The initial structure of the location database (LD) consists of:

1. The antenna table, shown by Figure 4.18 (Table 1 within the figure), stores all antenna/LED emitter coordinates and, in this instance, the relevant calibration parameters required, for example, the VLC Halo-Lens Compensation approach [21, 22]. Currently, VLP relies strongly on the assumed Lambertian properties of light sources. In practise, not all lights are Lambertian. To facilitate and benefit from the widespread deployment of VLC technology in numerous environments, measurements from non-Lambertian sources are analysed, and a novel calibration VLC halo-lens compensation technique was developed that enables high-accuracy positioning in a wider setting [21, 22].

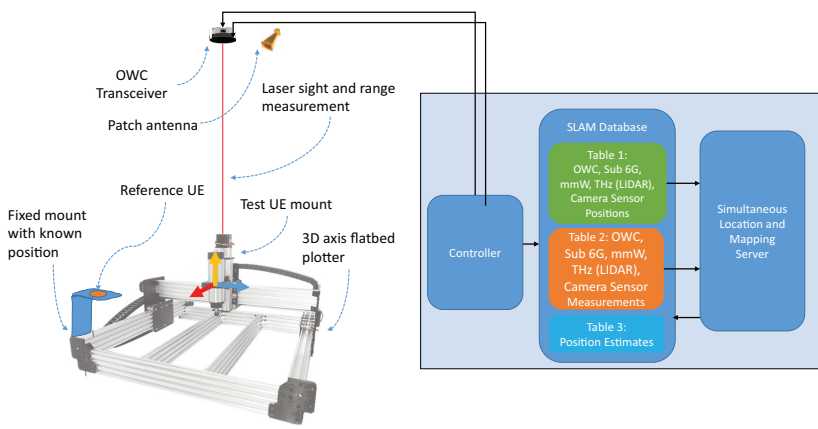

Figure 4.18. SLAM database and server system.

2. The measurement table, shown in Figure 4.18 (Table 2), stores all the latest measured location parameters obtained by the RAN. Here, we illustrate the OWC-RSS, sub-6GHz-TdoA, mmWave AoA, and eventual THz (LIDAR) and camera components. Each dataset (row) pertains to a singular UE with an appointed ID and timestamp of the measurement acquisition instant.
3. The estimates table, shown in Figure 4.18 (Table 3), is where the processed position estimates are stored. For data fusion applied later in the location server (LS), the states to be stored in the estimates table must be consistent with the states of the target applied to the location server. This enables the previous UE state estimates to be used within the Kalman filter as priory data. Asynchronous sampling of range-based measurements is known to have negative impacts on localization performance. Various asynchronous sampling localization techniques (ASLT) exist to mitigate these effects. The exact suitability of such solutions is not evident, due to their additional processes, subsequent complexity, and increased costs. Extensive simulations were conducted to demonstrate the effectiveness of ASLT under variable sampling latencies, sensor measurement noise, and target trajectories. These draw attention to the computational trade-off and lead to the development of a novel solution achieving optimal localization performance with a significant energy reduction of over 50% [22].

4.2 Enhancing Connectivity

4.2.1 Positioning and Position-aided Communication in Distributed Access Architectures

Envisioned interactive applications foresee that physical and virtual worlds will get blended, as introduced in Chapter 2. This requires for wireless connectivity support providing "real-time" and "real-space" functionality; the differences should be unnoticeable to the human and the potential machines and applications. Distributed access architectures are key candidates to provide this. For example, RadioWeaves technology is being developed to that end, presenting a platform of interconnected communication and computation resources [9].

Position information in these networks can play a double role:

1. It is directly required to enable novel applications in professional and care environments, entertainment, including gaming, and personal and home spaces. Clear examples include tracking and location-based services, as well as robotic applications in industrial environments and extended reality (XR) applications. The analysis of diverse use cases indicates that an accuracy of 1–0.1 m is required for many applications [23].

2. Position information can support wireless communication and power transfer functionality. For the latter, location information enables beamforming solutions, which can greatly benefit the efficiency of the transfer [24]. Furthermore, in the pursuit of ultra-reliable communication, position information can be exploited to anticipate bad connections and support "break before make" decisions.

Different device classes [23] have been categorized for nodes that will need to be positioned in the same environment. The selection of position-related measurements will strongly depend on the capabilities of these devices. In particular, the positioning of low-power devices without any battery or with only limited energy storage relies on wireless charging, which poses stringent limits.

Distributed architectures hosting a very large number of antennas offer hyper-diversity that can be exploited well to extract both accurate and precise position information. Accuracy is most often related when specifying requirements and algorithmic progress are reported. However, precision, which is a measure for variations on the accuracy and also quantifies bad outliers, is also an essential performance measure, in particular when reliability is important. A distributed deployment is of particular interest in this regard, as it can support the "zero-outage."

The distributed architectures also enable location-aware proactive redundancy for guaranteed ultrafast exchange of critical data. Cell-free access is being deployed to simultaneously sustain links to multiple arrays [25]. It is expected that distributed compute-connectivity infrastructures will be an essential part of the anticipated heterogeneous 6G networks, e.g., in the context of Industry 4.0 and in smart home and care environments [23]. A sudden bad connection to one array will always be covered in advance by another array without a latency penalty. The locations of devices were tracked, and information was used to provide ultra-robustness on critical links. Learning of the environment will support an optimal allocation of array resources to prevent retransmissions and link outages.

Adequate positioning techniques that can offer both good accuracy and good precision in distributed architecture open an opportunity to address the requirements of many novel applications mentioned as drivers for 6G [23]. Techniques leveraging on distributed resources will extract information from both LoS links and multipath reflections. Therefore, it is essential to characterize and model the propagation environment in distributed architectures hosting a very large number of antennas. Novel experimental campaign-based channel modelling work is being conducted. Algorithmic development exploits the ultra-wide aperture and near-field properties (in the sense of being within the Rayleigh distance) of the signals. Furthermore, the hypothesis that location and environmental awareness allow for a large-scale predictability of the channel state information and thus an

optimization of the efficient exploitation of the available hyper-diversity is confirmed in the first instance in the context of initial access [24].

4.2.2 Sub-6GHz, mmWave, and sub-THz RT Model and its Verification from Measurements and Applications Within Digital Twin of Factory for 6G

4.2.2.1 Construction of digital network twins in factory environments for access optimizations

6G envisions the integration of novel spectrum bands to support the development of ubiquitous smart wireless communications in industrial scenarios. Future industrial tasks and services rely on the simultaneous utilization of sub-6 GHz, mmwaves, sub-THz, and OWC [26]. The free blocks of spectrum available at THz and OWC enable the implementation of high-data-rate wireless links with enhanced capacity, latency, and with an unprecedented level of accuracy and resolution in sensing applications. Therefore, reliable channel models are of exceptional importance for the design, performance evaluation, standardization, and deployment of future 6G networks.

However, the development and parametrization of a single model covering such a wide spectrum of frequency bands and applications is challenging in multiple aspects. Localization and imaging applications require a precise correspondence between the geometrical properties of the propagated paths and the locations of users and scatterers. Moreover, testing heterogeneous localization methods, based on the combination of methods in different bands, requires models with consistency not only in the spatial domain, but also in the frequency domain: the scatterers must be in the same position for the different simulated bands [27, 28]. Therefore, models with deterministic components, such as RT, are more appropriate for these applications, since they allow simultaneous simulations at different frequencies with a precise geometrical representation of the environment in the propagation parameters of the paths. Nonetheless, the comparability of the results with reality depends on the complexity of the RT map/model. Thus, obtaining an accurate RT model with a high level of detail and a large number of objects is of crucial importance.

Therefore, a precise RT model was obtained from point cloud data from extensive 3D laser scans in an arbitrary industrial scenario, in which multiband RF measurements were also conducted simultaneously for propagation characterization [29] and calibration and verification of the model at sub-6 GHz and mmWave [30]. In addition, simultaneous sub-6 GHz, mmWave, sub-THz, and OWC measurements will be conducted for verification purposes in the future. The ultimate goal of this model is to perform realistic analysis on different algorithms

for sensing, localization, multi-band, and sensor-aided beamforming based on the different properties of this digital twin of the environment [31].

4.2.2.2 Channel modelling for heterogeneous networks and joint communications and sensing applications

From point cloud to RT simulations

The methodology to generate the RT model is summarized in Figure 4.19.

Two different scanners were used according to the size of the object/environment: the Leica BLK 360 for the macro scenario and the hand-held scanner Artec Leo for the machines and other details. The macro scenario was scanned in multiple positions, as shown in Figure 4.20, and the data were later combined using special tags that were placed in the environment.

The CAD model was obtained by reconstructing the surfaces out of the points. Once all the points from the different scans are merged, the surfaces are reconstructed with basic shapes out of polygons that can be interpreted by the RT tool. Figure 4.21 shows the level of detail on the CAD model. Finally, material-dependent electromagnetic properties are assigned to each surface to have an accurate calculation of the RF components at different frequencies with the RT tool.

Model validation with RF measurements

Simultaneously with the point-cloud scans, ultrawideband multiband RF measurements at sub-6 GHz, 30 GHz, and 60 GHz were conducted in the same area. These measurements have been used, as shown in Figure 4.22(a)–(c), to validate the RT model in the time-delay and angular domains. In the latter case, (c) shows the measured power at the different scanning angles (with 30° half power bandwidth (HPBW) horn antennas) at the TX side and the direction of the simulated paths,

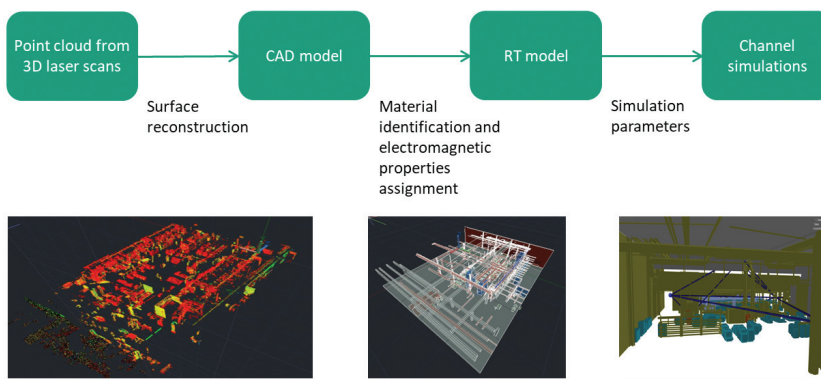

Figure 4.19. Processing methodology from point-cloud scans to RT models and simulations.

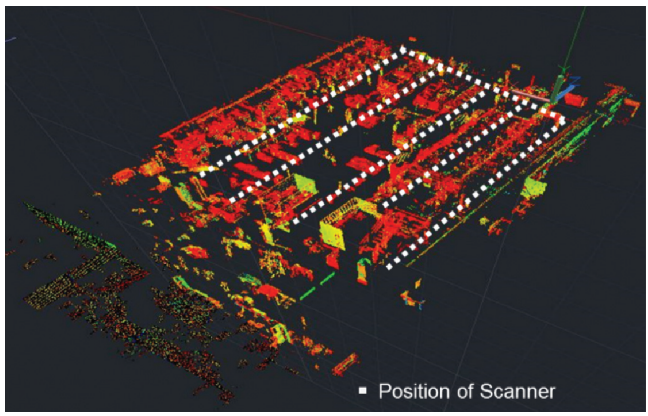

Figure 4.20. Point-cloud scanning positions.

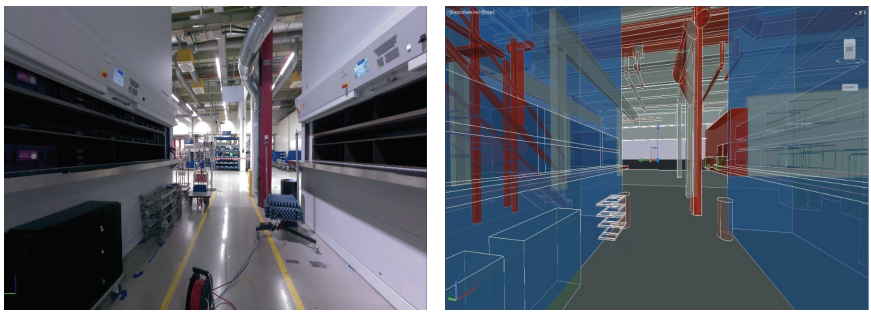

Figure 4.21. Picture of one of the corridors in the scenario and CAD model after surface reconstruction.

showing a high correlation between the density of the simulated path and the measured power.

After the RT model was validated, the simulations can be used to assist the interpretation of the measurement results by identifying scatterers and propagation mechanisms, as shown Figure 4.22(d).

A digital twin is a digital representation of a real object or process. In this case, the digital twin corresponds to the physical environment of a particular industrial scenario of interest. This model is used with RT to obtain different CIRs or RF parameters such as received power, delay spread, etc. that can be used in different tasks such as facilitating localization or the beam-steering process at high frequencies.

4.2.2.3 Applications of digital twins

However, one of the key requirements for digital twin components is their real-time representation or an acceptable update rate capability in order to tackle changes in high-dynamic environments in a factory.

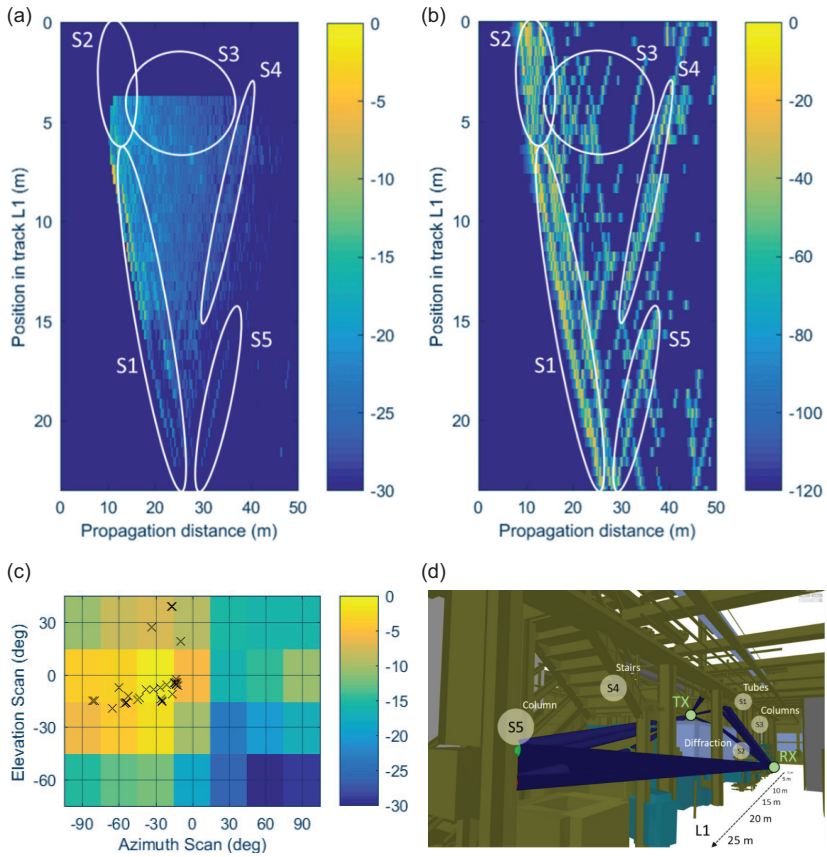

Figure 4.22. Power delay profiles of different RX positions over a line from (a) RF measurements at 6.75 GHz and (b) RT simulations. (c) Measured power azimuth/elevation profile and direction of the simulated paths in the RT model. (d) Identification of scatterers and propagation mechanisms.

An example of the latter case is that, given the location of the UE, RT can be used to determine the visibility condition or to estimate the pointing direction from the BS of a beam-former at mmWave or sub-THz, minimizing the training overhead.

4.2.3 Enhanced Connectivity with Channel Knowledge Map

Sensing to enhance communication services

A channel knowledge map (CKM) is a site-specific database containing transceiver locations and channel-related information that can be utilized to improve environmental awareness and improve CSI acquisitions. CKM is, therefore, critical to achieving high capacity, ultra-low latency, and ultra-massive connectivity in 6G networks. CKM can provide vital parameters of the wireless channels without requiring channel training. It is also possible to reduce training overhead in

large MIMO systems by advancing localization and environmental awareness. The authors in [32] examined environment-aware beamforming for RIS-aided communication enabled by the CKM, which does not require online training. In the simulation, CKM in active/passive beamforming led to significant rate improvements over training-based beamforming, and it also proved to be robust against UE location errors.

Together with CSI, dynamic blockage information from sensing services can also be useful for enhancing the communication performance, especially at high frequencies where the signal could be affected by the poor propagation environment with high path loss. To realize context information-assisted communications, the BS could potentially predict the position of UE and blockers with advanced sensors and localization techniques, and this information could be useful for dynamic blockage avoidance. Moreover, channel variance issues could be mitigated by using the recently proposed concept of predictor antenna (PA) [33]. PA system refers to a setup with two groups of antennas deploying on the top of a vehicle, where the front antennas (called PAs) sense and report back the CSI to the BS. Then, the receive antenna(s) (RA(s)) following behind the PAs could use the CSI from PAs when they reached the same positions as the PAs. In this way, the quality of CSI is improved, leading to better system performance. In [34], focusing on highway scenario, the PA concept was incorporated into a large-scale cooperative PA (LSCPA) setup with cooperative communications among BSs and utilize the information provided by different vehicles to avoid not only temporal blockages but also the CSI outdating. Results summarized in [32] indicate that the E2E throughput for a given time slot of the network can be improved by 32% using context information in the form of coarse localization and trajectory information, whereas with highly accurate localization and trajectory information, reliable CSI can be obtained with the PA concept, resulting in a 335% gain.

4.3 Joint Communication and Sensing

4.3.1 Introduction

JCAS is are already one of the main differentiators of the 6G vision with respect to 5G communication systems. While sensing includes positioning, it will also encompass novel functionalities that are not present in 5G, which in turn may lead to new services. Supporting these services will have architectural implications. This section will discuss these novel types of sensing, the services they may enable, and the implications for the 6G architecture. In addition, recent developments towards the practical implementation of joint communication and sensing will be detailed.

4.3.2 Sensing as a Service

The term sensing is often reduced from its broader definition (detection of events, measuring changes in the environment of physical properties) to mean radar-like sensing. However, sensing can also cover channel estimation, radio frequency sensing, spectroscopy, weather monitoring, and any downstream processes that rely on sensing data.

4.3.2.1 Technical concept

Radar-type sensing

Radar-type sensing can be classified into three categories: monostatic sensing, bistatic sensing, and positioning as sensing, with illustrations shown in Figure 4.23.

Monostatic sensing is an extensively studied topic in JCAS, where the transmitter and the receiver are co-located (e.g., radar, as shown in Figure 4.23(a)) and where the transmitted signal is reflected by surrounding objects or targets and then processed at the receiver. If the transmitter and the receiver are located at different places, it is called bistatic sensing, as shown in Figure 4.23(b). In these two scenarios, the receiver can estimate the position of the incidence point that reflects the signal (e.g., buildings, cars, bicycles, and pedestrians) and map the surrounding environment (mainly passive objects). In contrast, the concept of positioning as sensing refers to estimating the position of a connected device directly (i.e., UE) using signals from multiple anchors (shown in Figure 4.23(c)), with examples such as the global positioning system (GPS), ultra-wideband (UWB) positioning, and 5G positioning. The mentioned scenarios can also be combined. For example, when a UE with an unknown position is involved in bistatic sensing (e.g., one BS and one UE instead of two BSs), this becomes a SLAM.

Sensing involves several processing steps, some of which can be optimized in a closed-loop tracking scenario to progressively improve the sensing performance over time: (i) signal design, (ii) signal detection and acquisition, (iii) channel parameter estimation, and (iv) position estimation. The task of signal design could be

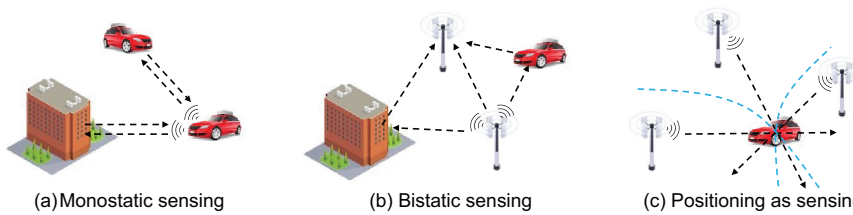

Figure 4.23. Illustration of three categories of sensing. (a) Sensing the environment with a vehicular radar. (b) Sensing the environment with two BSs. (c) Positioning of a vehicle with three BSs.

performed in time, frequency, and space to enhance sensing performance based on a priori knowledge of the environment obtained through position estimates in previous measurement epochs [35]. The designed signal is transmitted over the radio channel and acquired at the receiver, which then performs synchronization, phase noise tracking, and filtering. The sampled signal is applied to a parametric channel estimation routine, which returns estimates of ToA, AoD, AoA, and Doppler of the LoS path and possibly MPCs [36]. The channel parameters are provided for the localization, mapping, or tracking routine. This routine aims to solve the inverse problem of inferring the state of the UE (i.e., location and orientation) or the environment from the estimated channel parameters. In monostatic sensing, the transmitted data could be known at the receiver due to being co-located on the same hardware, which enables sensing using communication payload data. However, in bistatic sensing and positioning, pilot (reference) signals are needed, and there is a trade-off between communication and sensing resources.

In general, the sensing estimation accuracy depends on a variety of factors, which can be summarized as follows: (i) resolution, (ii) SNR, (iii) sensing scenario, and (iv) model mismatch. To estimate the parameters of a signal path during the channel estimation, the path should be resolvable (separable) in at least one domain among delay, AoD, AoA, or Doppler. However, even under sufficient resolution, the received signal may be weak and limit the performance, which can be determined by the transmit power, path loss, the reflection coefficient of the object, etc. In addition, the sensing scenario (deployment of transmitters and receivers, operating frequency, etc., which have implications on blocking, scattering, or molecular absorption characteristics) and the mobility of objects and users (the coherent processing duration of the waveforms will be limited) play a vital role. Finally, unmodelled effects due to radio hardware impairments or propagation effects will lead to reduced localization and sensing performance, which can have severe impacts in applications with stringent accuracy requirements.

Consequently, offline sensing system design (e.g., hardware selection and deployment), online optimization (e.g., signal design), and signal processing algorithms (taking into account the model mismatch or not) constitute essential ingredients to guarantee an acceptable level of performance for a sensing system.

Non-radar type sensing

Typical sensing methods for using communication infrastructure try to mirror a radar. In these methods, focus is on detecting the target and estimating its parameters such as velocity, range, etc. However, there are sensing use cases where the focus is not on range and Doppler but on other aspects, such as sensing weather, human activity, local environment, etc. Figure 4.24 illustrates the communication infrastructure for non-radar type of sensing.

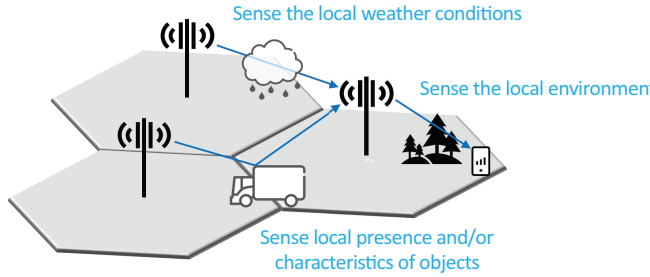

Figure 4.24. Radar and non-radar type of sensing using mobile networks.

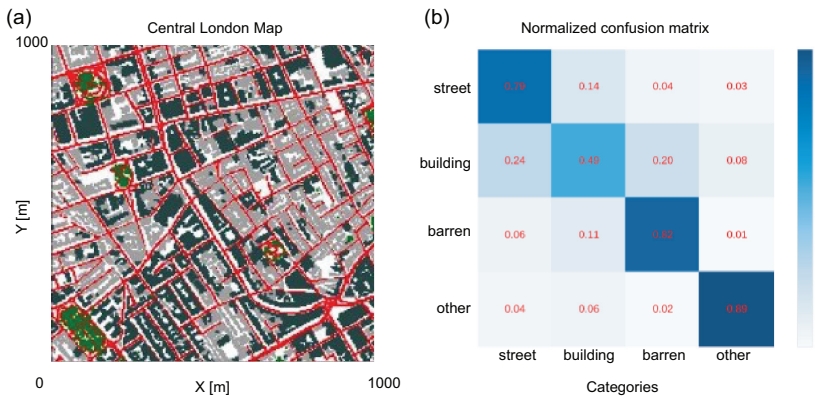

Figure 4.25. (a) Central London map with different landscapes shown in different colours. (b) Classification accuracy denoted via confusion matrix for landscape sensing algorithm discussed in [37].

4.3.2.2 Use of sensing information in services

Landscape sensing and contextual sensing (incl. weather monitoring)

Landscape sensing methods identify the macro-environment around the UE, such as forests, streets, buildings, water body, etc. It can aid in several scenarios in RAN automation such as tailoring the signal to the UE from the BS. The landscape sensing methods proposed in [37] detect the UE landscape using measurements from the central London metropolitan area (refer to Figure 4.25(a)). Figure 4.25(b) shows the classification accuracy achieved using the methods proposed in [37]; here, landscape categories such as those that denote "street," "building," "barren landscapes," and "other" categories can be applied.

Contextual sensing is another type of non-radar type of sensing that deals with identifying the target context and aiding in the higher-level tasks. For example, a fall detection in an assisted living scenario can trigger an emergency call to the hospital. In [32], the authors proposed active sensing where target-UE uses its communication capability to share its inertial sensor values with the edge-server in the

BS. Using these inertial sensor values, an AI agent on the edge server will identify the human activity.

Sensing to optimize factory environments

The digitalization within factories is progressing, but the integration of the digital and physical worlds still faces many challenges. Localization, sensing, and integrated communication will play an important role, and next-generation mobile communication systems can support the Industry 4.0 vision in a great manner. Sensing the environment and creating a digital twin of objects and layouts of the building help digitalize the factory environment. Localization of mobile units such as AGVs or assets (respectively products) within and outside of the factory allows for seamless tracking and analytics of business flows. Errors in production processes can be detected early, and inefficient flows can be optimized. The evaluation of the current location and communication requirements of mobile units is examined and optimized bidirectionally. Mobile units can take routes that may be a little longer but more efficient in regard to communication requirements (throughput, latency, etc.). Next-generation mobile networks with integrated sensing capabilities will be even more valuable if sensor fusion with existing localization and sensing technologies (e.g., camera, LIDAR, or UWB-based) is able by offering open interfaces.

4.3.2.3 Architectural implications of sensing as a service

Signal resource allocation

To implement sensing on the OFDM transceivers, the sensing resources need to be periodically allocated, as shown in Figure 4.26. Typical sensing (radar-type) use cases can be mapped to the requirements on the range resolution, maximum unambiguous range, velocity resolution, and unambiguous velocity. These requirements put constraints on the OFDM waveform, specifically on periodicity, symbol duration, and frame time, as illustrated in Figure 4.26. In [38], the sensing overhead for a traffic sensing use case was computed, considering a range resolution of 0.5 m, a maximum unambiguous range of 100 m, a velocity resolution of 0.5 m/s, and unambiguous velocity in the range of [−20 to 20] m/s, for realizing traffic sensing use case, and showing that this will result in an overhead of 2.7% for a mmWave deployment with numerology, centre frequency, subcarrier spacing, and bandwidth of 28 GHz, 120 kHz, and 300 MHz, respectively.

Network, spectrum, and hardware requirements

To sense target in mono-static way, the transceiver must simultaneously transmit and receive signals; this creates a full duplex requirement on the communication infrastructure. Such a full-duplex-capable transceiver requires a high level of self-interference cancellation, which is very challenging. This can be overcome by using

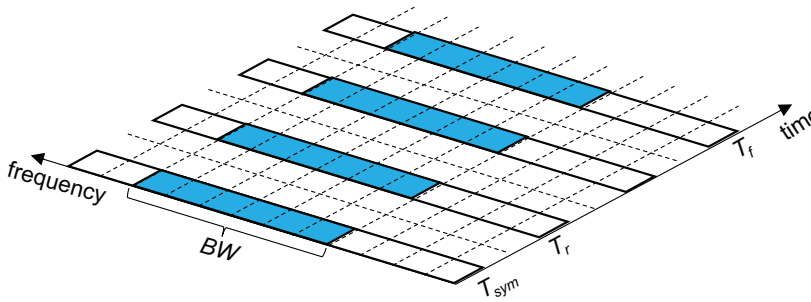

Figure 4.26. Sensing overhead in OFDM frame.

bi-static or multi-static sensing; however, these methods require a high level of synchronization between the co-operating BSs, which is very challenging to achieve.

Though large bandwidth and high frequency of operation are beneficial from a sensing perspective as they can enable very high range and angle resolutions, they come with a cost of very limited coverage and expensive hardware. In contrast, the lower-frequency spectrum provides much wider coverage. Depending on the accuracy and coverage requirements for the use case spectrum, these need to be carefully chosen.

Services in the 6G ecosystem

Sensing the environment will be a completely new feature, and the capabilities are gaining more relevance as localization becomes more accurate and reliable. Especially indoors, where no GPS is available, the next-generation mobile networks can add high impact on certain applications. But with these developments, the service offering from pure communication service is broadened, and the stakeholders and users' groups might grow. The complexity of offering multiple services will be challenging. The configuration and even the usage of these services should be flexible. In some scenarios, all capabilities will be needed at the same time, which might even require an integrated approach. The next-generation mobile networks should be as flexible as possible in each phase of the lifecycle (planning, analysis, design, development, testing, implementation, and maintenance). Especially in indoor environments, the requirements can change over time, and it might be necessary to include new hardware, even from third-party vendors to enhance the service quality. Also, accessing sensing data in a standardized manner at various processing stages (from raw to finalized contextual data) is beneficial to allow an ecosystem to flourish and enable, for example, a truly seamless sensor fusion between different sensing and localization technologies. Privacy might become more sensitive for two reasons. First, as localization information becomes more accurate, misusage can damage or harm people and institutions much more severely, and secondly, sensing people

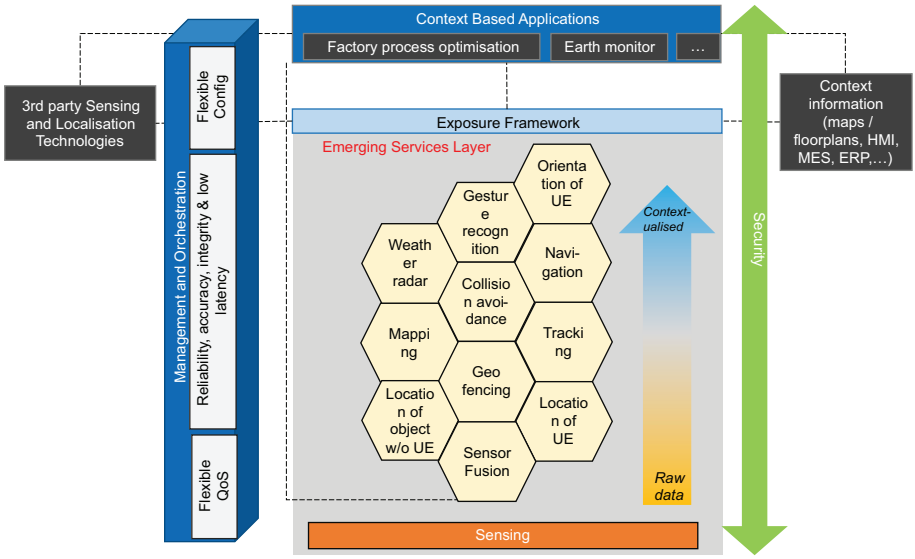

Figure 4.27. Location-based services ecosystem from sensing perspective.

(radar-like) and detecting the presence of humans pose a new category of privacy concerns, especially if, with pattern analysis, the identification of this detected person can be deduced. If critical use cases are built on top of sensing and localization data, the sensing data itself must be secured and verified by next-generation mobile network mechanisms.

New services may emerge based on sensing and localization capabilities, or existing services may integrate into the next generation of mobile network capabilities. A very straight-forward synergy between services is to enhance communication based on the current location. The farther away a service resides in Figure 4.27 from pure and raw sensing data, the more context information and classification of data are required by the service.

4.3.3 Joint Communication and Sensing in Practice

When developing new technologies, there is always a big step to go from a theoretical idea to showing that it works in practise. In Figure 4.28, the results from some initial JCAS tests are shown. In this example, a bi-static setup operating at 69 GHz is used. The signal transmitted is a 400 MHz-wide OFDM signal with 960 kHz subcarrier spacing. In the setup, there is a reflective wall and a person (wearing a tin foil hat to enhance reflections) that should be detected. Both the transmitter and receiver consist of a 1 × 16-element phase array, where the transmitter uses 50 different beams and the receiver uses 56 different beams, both in the range ±45°. In the bottom left plot, the RSS is plotted as a function of the beam indices of the

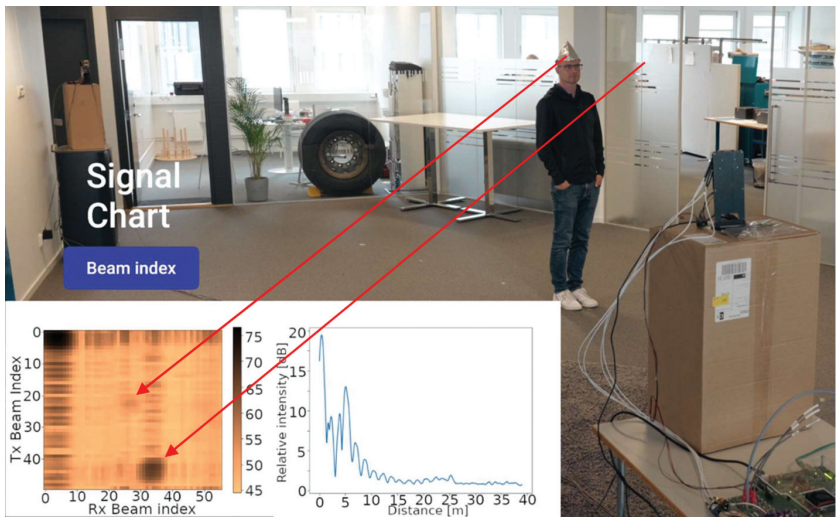

Figure 4.28. Initial demonstrations of JCAS using a bistatic setup at 69 GHz.

transmitter and receiver. At indices 0,0, the strongest response is found, and that corresponds to the LoS channel. In addition, there are two more blobs indicated by the red arrows, one originating from reflections at the wall and the other from the person in the picture. In the right plot, the distance to the targets is calculated based on the channel estimation. The distance indicated is relative to the LoS distance, meaning that the 0 m peak is due to the LoS channel, the peak at 5 m is caused by the wall, and the small peak at 2 m is caused by the person. For a more detailed description of the demonstration and more pictures, see [32].

4.4 Conclusions

The global impact of the existing global positioning system (GPS) has transformed the lives of many people with many new applications that use outdoor location information, which has impacted people's lives in many different ways, such as: (1) find your path, (2) avoiding traffic, (3) tracking your phone or child's phone, (4) finding the nearest place such as restaurant, (5) finding places such as schools & colleges, (6) track stolen phone, (7) preventing car theft, (8) tracking for law enforcement, (9) discover unknown places, and (10) find nearby places. It is expected that indoor and outdoor location systems with an accuracy of millimetres, which cannot be performed by GPS due to the building obscuring the direct line of site to GPS satellites, will similarly transform the lives of many people by inspiring many new indoor and outdoor applications, which will have a global impact on people's lives in many different new ways in many different verticals. Furthermore

the introduction 6G JCAS capabilities will allow the spatial sensing of the environment since by measuring the delay of the return echo in the line-of-sight path between the transmitter and object, the distance to the object can be calculated and therefore its position and velocity. This is very useful information for not only appraising the LoS/NLoS radio transmission in which mMIMO dart-like beams propagate but also sensing object for collision avoidance, proximity sensing and location from landmark sensing.

References

[1] *OS1 Ultra-Wide View High-Resolution Imaging Lidar*, Ouster Specification OS1 rev. 7 v.3.0, 2023. Accessed: April 6, 2023. [Online]. Available: https://data.ouster.io/downloads/datasheets/datasheet-rev7-v3p0-os1.pdf.

[2] *OS2 Ultra-Wide View High-Resolution Imaging Lidar*, Ouster Specification OS2, rev 6, v2.4.x, 2022. Accessed: April 6, 2023. [Online]. Available: https://data.ouster.io/downloads/datasheets/datasheet-rev06-v2p4-os2.pdf.

[3] 6G BRAINS, "D2.1 Definition and Description of the 6G BRAINS Primary Use Cases and Derivation of User Requirements," July 2021. Accessed: April 6, 2023. [Online]. Available: https://ec.europa.eu/research/participants/documents/downloadPublic?documentIds=080166e5f5607765&appId=PPGMS.

[4] Hexa-X, "D3.1 Localisation and sensing use cases and gap analysis," Dec. 2021. Accessed: April 6, 2023. [Online]. Available: https://ec.europa.eu/research/participants/documents/downloadPublic?documentIds=080166e5e648d02a&appId=PPGMS.

[5] 6G BRAINS, "D3.1 3D Laser measurement of one factory at Bosch with 3D cloud scanner and 3D hand scanner," Sep. 2021. Accessed: April 6, 2023. [Online]. Available: https://ec.europa.eu/research/participants/documents/downloadPublic?documentIds=080166e5e2a9ad6f&appId=PPGMS.

[6] G. Eappen, J. Cosmas, T. Shankar, A. Rajesh, R. Nilavalan, and J. Thomas "Deep learning integrated reinforcement learning for adaptive beamforming in B5G networks," In *IET Communications*, Sept. 2022. Accessed: April 6, 2023. [Online]. Available: https://doi.org/10.1049/cmu2.12501.

[7] 6G BRAINS, "D6.1 Technical Specification of the 3D Location Architecture," Jan. 2022. Accessed: April 6, 2023. [Online]. Available: https://ec.europa.eu/research/participants/documents/downloadPublic?documentIds=080166e5f561136a&appId=PPGMS.

[8] S. S Das and R. Prasad, *Orthogonal Time Frequency Space Modulation OTFS a waveform for 6G*, New York, NY, USA, River Publishers, September 1, 2022,

eBook ISBN9781003339021, Accessed: April 6, 2023. [Online]. Available: https://doi.org/10.1201/9781003339021.

[9] L. Van der Perre, E. G. Larsson, F. Tufvesson, L. D. Strycker, E. Björnson and O. Edfors, "RadioWeaves for efficient connectivity: analysis and impact of constraints in actual deployments," In *2019 53rd Asilomar Conference on Signals, Systems, and Computers*, pp. 15–22, Pacific Grove, CA, USA, 2019, doi: 10.1109/IEEECONF44664.2019.9048825.

[10] T. Wilding, S. Grebien, E. Leitinger, U. Mühlmann and K. Witrisal, "Single-Anchor, Multipath-Assisted Indoor Positioning with Aliased Antenna Arrays (Invited Paper)," In *2018 52nd Asilomar Conference on Signals, Systems, and Computers*, pp. 525–531, Pacific Grove, CA, USA, 2018, doi: 10.1109/ACSSC.2018.8645163.

[11] T. L. Hansen, M. A. Badiu, B. H. Fleury and B. D. Rao, "A sparse Bayesian learning algorithm with dictionary parameter estimation," In *2014 IEEE 8th Sensor Array and Multichannel Signal Processing Workshop (SAM)*, pp. 385–388, A Coruna, Spain, 2014, doi: 10.1109/SAM.2014.6882422.

[12] 5G-CLARITY, "D2.3 Primary System Architecture Evaluation," July 2021. Accessed: April 6, 2023. [Online]. Available: https://ec.europa.eu/research/participants/documents/downloadPublic?documentIds=080166e5f30947a2&appId=PPGMS.

[13] A. S. Stordal, H. A. Karlsen, G. Naevdal, H. J. Skaug, and B. Valles, "Bridging the ensemble kalman filter and particle filters: the adaptive Gaussian mixture filter," In *Computational Geosciences*, pp. 293–305, 2011.

[14] D. Alspach and H. Sorenson, "Nonlinear Bayesian estimation using Gaussian sum approximations," In *IEEE transactions on automatic control*, vol. 17, pp. 439–448, 1972.

[15] F. Gustafsson, "Particle filter theory and practice with positioning applications," In *IEEE Aerospace and Electronic Systems Magazine*, vol. 25, pp. 53–82, 2010.

[16] M. Goodarzi, V. Sark, N. Maletic, J. Gutiérrez, G. Caire, and E. Grass, "DNN-assisted Particle-based Bayesian Joint Synchronization and Localization," In *IEEE Transactions on Communications*, vol. 70, no. 8, July 2022.

[17] R. O. Schmidt, "Multiple emitter location and signal parameter estimation," In *IEEE Trans. Antennas Propag.*, vol. AP-34, no. 3, pp. 276–280, Mar. 1986.

[18] 5G-CLARITY, "D4.2 Validation of 5G-CLARITY SDN/NFV Platform, Interface Design with 5G Service Platform, and Initial Evaluation of ML Algorithms," July 2021. Accessed: April 6, 2023. [Online]. Available: https://ec.europa.eu/research/participants/documents/downloadPublic?documentIds=080166e5f309449b&appId=PPGMS.

[19] J. Heaton, *Introduction to neural networks with Java 2nd edition.*, Heaton Research Inc. Oct. 1, 2008.

[20] S. Boyd and L. Vandenberghe, *Convex optimization*, Cambridge university press, 2004.

[21] B. Meunier, J. Cosmas, K. Ali, N. Jawad, G. Eappen, W. Li, and H. Zhang "Visible Light Positioning with Lens Compensation for Non-Lambertian Emission," In *IEEE Transactions on Broadcasting*, vol. 69, no. 1, pp. 289–302, March 2023.

[22] B. Meunier "Wireless Indoor Localisation within the 5G Internet of Radio Light," Ph. D. Thesis, Brunel University, London, March 2022.

[23] REINDEER, "D1.1 Use case-driven specifications and technical requirements and initial channel model," Sep. 2021. Accessed: April 6, 2023. [Online]. Available: https://ec.europa.eu/research/participants/documents/downloadPublic?documentIds=080166e5e2ac056c&appId=PPGMS.

[24] B. Deutschmann, T. Wilding, E.G. Larsson, and K. Witrisal, "Location-based Initial Access for Wireless Power Transfer with Physically Large Arrays," In *2022 IEEE International Conference on Communications Workshops (ICC Workshops)*, 16–20 May 2022.

[25] REINDEER, "D2.1 Initial assessment of architectures and hardware resources for a RadioWeaves infrastructure," Jan. 2022. Accessed: April 6, 2023. [Online]. Available: https://ec.europa.eu/research/participants/documents/downloadPublic?documentIds=080166e5e7bcfeeb&appId=PPGMS.

[26] European Commission, "Bring Reinforcement-learning Into Radio Light Network for Massive Connections (6G BRAINS)," CORDIS, 2023. Accessed: April 6, 2023. [Online]. Available: https://cordis.europa.eu/project/id/101017226.

[27] D. Dupleich, R. Müller, M. Landmann, E. Shinwasusin, K. Saito, J. Takada, J. Luo, R. Thomä, and G. del Galdo, "Multi-Band Propagation and Radio Channel Characterization in Street Canyon Scenarios for 5G and Beyond," In *IEEE Access*, vol. 7, pp. 160385–160396, 2019.

[28] D. Dupleich, R. Müller, M. Landmann, J. Luo, G. Del Galdo and R. S. Thomä, "Multi-band Characterization of Propagation in Industry Scenarios," In *14th European Conference on Antennas and Propagation (EuCAP)*, Copenhagen, Denmark, 2020.

[29] D. Dupleich, N. Han, A. Ebert, R. Müller, S. Ludwig, A. Artemenko, J. Eichinger, T. Geiss, G. Del Galdo, and R. Thomä, "From Sub-6 GHz to mm-Wave: Simultaneous Multi-band characterization of Propagation from Measurements in Industry Scenarios," In *16th European Conference on Antennas and Propagation (EuCAP)*, Madrid, Spain, 2022.

[30] H. Niu, D. Dupleich, Y. Völker-Schöneberg, A. Ebert, R. Müller, J. Eichinger, A. Artemenko, G. Del Galdo, and R. Thomä, "From 3D Point Cloud Data to Ray-tracing Multi-band Simulations in Industrial Scenario," In *2022 IEEE 95th Vehicular Technology Conference: (VTC2022-Spring)*, Helsinki, 19–22 June 2022.

[31] 6G BRAINS, "D6.2 3D Location Simulation Models and Lab Prototypes," Jan. 2023.

[32] Hexa-X, "D3.2 Initial models and measurements for localisation and sensing," Oct. 2022.

[33] H. Guo, B. Makki, D. T. Phan-Huy, E. Dahlman, M.S. Alouini, and T. Svensson, "Predictor antenna: A technique to boost the performance of moving relays," In *IEEE Communications Magazine*, vol. 59, no. 7, pp. 80–86, 2021.

[34] H. Guo, B. Makki, M. Alouini, and T. Svensson, "High-rate uninterrupted internet-of-vehicle communications in highways: Dynamic blockage avoidance and CSIT acquisition," In *IEEE Communications Magazine*, vol. 60, no. 7, pp. 44–50, July 2022.

[35] A. Kakkavas, H. Wymeersch, G. Seco-Granados, M. H. Castañeda García, R. A. Stirling-Gallacher, and J. A. Nossek. "Power Allocation and Parameter Estimation for Multipath-based 5G Positioning," In *IEEE Transactions on Wireless Communications*, vol. 20, no. 11, pp. 7302–7316, Nov. 2021.

[36] H. Chen, H. Sarieddeen, T. Ballal, H. Wymeersch, M. S. Alouini, and T. Y. Al-Naffouri, "A Tutorial on Terahertz-Band Localization for 6G Communication Systems," In *IEEE Communications Surveys & Tutorials*, vol. 24, no. 3, pp. 1780–1815, May. 2022.

[37] V. Yajnanarayana, D. Huang, D. Shrestha, Y. Geng, A. Behravan, and E. Dahlman, "AI Based Landscape Sensing Using Radio Signals," In *2021 IEEE 32nd Annual International Symposium on Personal, Indoor and Mobile Radio Communications (PIMRC)*, pp. 1–5, 2021, doi: 10.1109/PIMRC50174.2021.9569617.

[38] A. Behravan, R. Baldemair, S. Parkvall, E. Dahlman, V. Yajnanarayana, H. Björkegren, and D. Shresta, "Introducing sensing into future wireless communication systems," In *2022 2nd IEEE International Symposium on Joint Communications & Sensing (JC&S)*, pp. 1–5, 2022, doi: 10.1109/JCS54387.2022.9743513.